Supporting information

Intermediate and semi-volatility organic compounds (I/SVOCs) emission from Chinese Vehicles: volatility distribution, influencing factors, and implication for SOA formation

Yajun Wu[1†], Peiji Liu[1†], Yajie Wang[1], Xiaoguo Wang[2], Jing Zhang (✉)[2], Yan Liu[1], Jinsheng Zhang[1], Lin Wu[1], Ting Wang[1], Hongjun Mao[1], Jianfei Peng (✉)[1]

1 Tianjin Key Laboratory of Urban Transport Emission Research, College of Environmental Science and Engineering, Nankai University, Tianjin 300071, China

2 Tianjin Eco-Environmental Monitoring Center, Tianjin 300071, China

Supplementary Text

S1. Calculation of retention index (RI)

Compared to the similarity of mass spectrum matching (Match), R. Match performs a comparison by matching the spectrums from NIST reference to the samples. This approach helps eliminate interference caused by MS background noises and reduces the co-eluting impacts of overlapping species, thereby improving the reliability of the analysis outcomes (Lu et al., 2018; Song et al., 2023a). The retention index (RI) later served in differentiate isomers based on their one-dimensional retention time. If the retention indices of n-alkanes (Cn) are defined as n × 100, e.g., the retention index of C8 is 800, the RI value for species A, positioned between Cn and Cn + 1, could be determined using the equation below (Eq. (S1)) (Lu et al., 2018):

$$RI(A) = \left(\frac{t_A - t_{Cn}}{t_{Cn+1} - t_{Cn}} + n\right) \times 100 \quad , \quad \text{(S1)}$$

where t_A, t_{Cn} and t_{Cn+1} are the one-dimensional retention times of species A, C_n, and C_{n+1}, respectively.

✉ Corresponding authors
E-mail: zhangjing_gogo@126.com (J. Zhang); pengjianfei@nankai.edu.cn (J. Peng)
†These authors contributed equally to this work.

S2. Calibration for authentic standards and uncertainties of quantification procedures

Organic species were identified based on their ion fragmentation, retention time, and comparison with the NIST library. A total of 55 authentic standards were used. Multipoint calibration curves (n = 7) were generated using relative MS responses from standard dilutions of 5, 10, 25, 50, 100, 200, and 400 ng. Each concentration standard was tested twice to minimize measurement error. The actual calibrated quantities (ng) were determined using the standard curve along with the quantifier response. The RSD values for all VOC standards reported in this study were below 15%, and the R^2 values for all targeted I/SVOCs were higher than 0.95 (Table S4), demonstrating the robustness and accuracy of the quantification of S/IVOCs.

For speciation and quantification of I/SVOCs, species were measured either through compound-specific calibration using the standards or by associating ion chromatogram signals with those of calibration standards that share similar structures, polarities, and volatilities (Song et al., 2023b; Song et al., 2023c). Peaks corresponding to authentic standards were accurately identified. For compounds without authentic standards, identification was based on their elution sequence on two GC columns and their characteristic mass spectrum patterns. Experimental first retention times were converted to retention indices (RIs), which serve as essential parameters for assessing the volatility of organic compounds and classifying them into VOC, IVOC, and SVOC categories (Lu et al., 2018). Additional organic compounds were grouped into various chemical categories according to their respective volatility ranges. To handle the intricate data sets acquired from GC × GC–TOFMS, homologs were primarily determined using selected ion chromatograms (SICs) combined with retention index values. Surrogate compounds were employed for the semi-quantification of organics in the absence of specific standards (Song et al., 2023a)

Species without authentic standards were semi-quantified using surrogate compounds, either derived from n-alkanes within the same volatility range or from surrogates belonging to the same chemical class. Due to the differing MS behaviors of these compounds compared to surrogates, some uncertainty exists in the quantitative results. Thus, representative species among cyclo-alkanes, oxygenated compounds, and aromatics were selected. The difference in quantification between authentic and surrogate standards was used for uncertainty calculation. For every chosen standard species, a surrogate standard belonging to a similar chemical group and an n-alkane surrogate within an equivalent volatility range. The actual calibrated quantities (ng) are determined using the calibration curve along with the quantification signal. Semi-quantification values (ng) were determined using the total ion current responses from the standards and the surrogate standards. The variation in results for quantification and semi-quantification are determined with the equation below (Eq. (S2)) (Song et al., 2023a):

$$D\% = \frac{A_s - A_d}{A_d} \times 100\% \quad , \qquad \text{(S2)}$$

where, A_s and $A_d$represent the amounts determined through quantification and semi-quantification.

The overall uncertainty was evaluated based on the equation below (Eq. (S3)):

$$D_{total}\% = \sqrt{D_1^2 + D_2^2 + ...D_n^2} \quad , \qquad \text{(S3)}$$

where, D_1, $D_2 ...$ D_n represent the uncertainties associated with each standard.

For these species without authentic standards, the concentrations exhibited an overall uncertainty ranging from 21% to 57% in our study.

S3. The calculation of fuel-based EFs and double bond equivalents (DBE)

The mileage-based EFs described could be transformed into fuel-based ones based on fuel efficiency and fuel density, as expressed in Eq. (S4):

$$EF\_fuel = \frac{EF\_mileage}{fuel\_density \times fuel\_efficiency} \quad , \qquad \text{(S4)}$$

In this study, average fuel efficiencies of 0.0787 L/km for gasoline and 0.075 L/km for diesel were used. The fuel density was taken as 0.74 g/mL for gasoline and 0.85 g/mL for diesel, respectively (Zhang et al., 2016).

The double bond equivalents (DBE), which indicate the degree of unsaturation of compound (Lin et al., 2018; Huo et al., 2021), were determined using the following formula (Eq. (S5)) for the elemental composition $C_cH_hO_oN_nS_s$:

$$DBE = \frac{2c+2-h+n}{2} \quad , \qquad \text{(S5)}$$

where, c, h, o, n and s denote the quantities of carbon (C), hydrogen (H), oxygen (O), nitrogen (N), and sulfur (S) atoms, respectively.

S4. the Bin o of I/SVOCs based on Zhao et al. (2014)

Speciated I/SVOCs were characterized using retention times, mass spectra, and their quantification was performed using authentic standards, including C7–C30 n-alkanes as well as 16 PAHs. The method developed by Zhao et al. (2014) was utilized to categorize organics into bins based on the retention times of C7–C30 n-alkanes. The approach proposed by Zhao et al. (2014) was utilized to categorize organics into bins based on the retention times of C7–C30 n-alkanes. The beginning and ending times of the chromatogram bin were defined by consecutive n-alkanes (Eqs. (S6) and (S7)):

$$t_{n,Bin-start} = \frac{t_{n-1}+t_n}{2} \quad , \qquad \text{(S6)}$$

$$t_{n,Bin-end} = \frac{t_n+t_{n+1}}{2} \quad , \qquad \text{(S7)}$$

where, n denotes the carbon count of n-alkane that corresponds to the center of the relevant chromatogram bin. The $t_{n,Bin-start}$ and $t_{n,Bin-end}$ respectively represent beginning and ending

times of chromatogram bin. The t_{n-1}, t_n, t_{n+1} correspond to the retention times of C_{n-1}, C_n, and $C_{n+1}$of n-alkanes, respectively.

S5. Analysis of gas adsorption artifacts in measurements of organics to filters

We referred to the methodology in previous studies, we introduced the parameter $K_{p,face}$and used the following equation to roughly quantify the extent of overestimation caused by gaseous organic adsorption on filters

$$Loss_{gas}\ (\%) = \frac{\sum c_{i,g} \times K_{p,face} \times A_f}{\sum c_{i,p} \times v} \quad , \qquad \text{(S8)}$$

$Loss_{gas}$ is the rate of gas adsorption onto filter (%);C_i represents the concentration in the gas-phase(μg/cm^3) and particle phase;$K_{p,face}$is the gas/filter partition coefficient (m^3·cm^{-2}), expressed as [ng sorbed per cm^2 of filter face]/ [ng per m^3 in the gas phase]; A_f refers to the cm^2 of filter face area(cm^2).

Supplementary Tables

Table S1 Detailed information of the Light-Duty Gasoline Vehicles (LDGV) and Light-Duty Diesel Vehicle (LDDV) employed in this study.

Test ID	Manufacture	vehicle type	Emission Standard	Model Year	Mileage (km)	Gross Mass (kg)	Fuel type	Aftertreatment Technologies	Fuel economy (L/100km)
1	Volkswagen	LDGV	China6	Jan-21	84561	1545	gasoline		5.8
2	Volkswagen	LDGV	China6	Jan-22	5642	1640	gasoline		6.7
3	Toyota	LDGV	China6	Mar-22	1120	1215	gasoline		5
4	Volkswagen	LDGV	China6	Dec-21	36000	1500	gasoline		6.6
5	Capgemini	LDDV	China6	Feb-22	35375	4495	Diesel	DOC + DPF + SCR	9.8
6	FAW	LDDV	China5	Jul-19	91720	4495	Diesel	DOC + DPF + SCR	9.9
7	Fukuda	LDDV	China6	Mar-22	53000	4495	Diesel	DOC + DPF + SCR	8.2
8	Ford	LDDV	China4	Feb-15	121230	3510	Diesel	SCR	10.1

Table S2 Thermal desorption (TD-100) method parameters used for this study.

Instrument	Items	Parameter setting
TD (Markes, TD-100, UK)	Flow path temp	180℃
	Tube desorb time	15 min
	Tube desorb temp	315℃
	Trap high	330℃
	Trap hold	5 min
	Pre-trap fire purge	1.0 min
	Carrier gas pressure	5psi

Table S3 GC×GC-TOF-MS method parameters used for this study.

Instruments	Modules	Parameter	Parameter setting
GGT 0620 GC×GC-TOF-MS （Guangzhou Hexin Instrument Co., Ltd., China）	Column		
		1D column	DB-5 ms (30 m × 0.25 mm × 0.25 μm, Agilent, USA)
		2D column	DB-17 ms (1 m × 0.18 mm × 0.18 μm, Agilent, USA,)
		Total run time	100min
		Carrier gas	He
		Inlet mode	Split
	Oven Temperature	Inlet Temp.	300℃
		Oven	40℃ (5 min), 5℃/min to 310℃ (5 min)
	Mass Spectrometry	Ionization	EI, 70 eV
		Transfer line Temp	300℃
		Mass range	35–600 m/z
		Acquisition rate	101 spectra s^{-1}
		Acquisition delay	4.5 min
		Ion Source Temp	250℃

Table S4 Information on the standard samples and the R^2 of calibration curves used for quantification in this study.

Compounds	Category	Subcategory	R^2	compounds	Category	Subcategory	R^2
Heptane	Alkanes	n-alkane	0.985	Naphthalene	Aromatics	PAHs	0.976
Octane	Alkanes	n-alkane	0.999	Acenaphthylene	Aromatics	PAHs	0.967
Nonane	Alkanes	n-alkane	0.99	Acenaphthene	Aromatics	PAHs	0.952
Decane	Alkanes	n-alkane	0.994	Fluorene	Aromatics	PAHs	0.99
Undecane	Alkanes	n-alkane	0.992	Phenanthrene	Aromatics	PAHs	0.965
Dodecane	Alkanes	n-alkane	0.991	Anthracene	Aromatics	PAHs	0.997
Tridecane	Alkanes	n-alkane	0.985	Fluoranthene	Aromatics	PAHs	0.979
Tetradecane	Alkanes	n-alkane	0.973	Pyrene	Aromatics	PAHs	0.987
Pentadecane	Alkanes	n-alkane	0.994	Chrysene	Aromatics	PAHs	0.976
Hexadecane	Alkanes	n-alkane	0.978	Benzo[b]fluoranthene	Aromatics	PAHs	0.999
Heptadecane	Alkanes	n-alkane	0.994	Benz[a]anthracene	Aromatics	PAHs	0.962
Octadecane	Alkanes	n-alkane	0.998	Benzo(k)fluoranthene	Aromatics	PAHs	0.952
Nonadecane	Alkanes	n-alkane	0.993	Benzo(a)pyrene	Aromatics	PAHs	0.955
Eicosane	Alkanes	n-alkane	0.996	Indeno(1,2,3-cd)pyrene	Aromatics	PAHs	0.947
Heneicosane	Alkanes	n-alkane	0.993	Dibenzo(a,h)anthracene	Aromatics	PAHs	0.951
Docosane	Alkanes	n-alkane	0.988	Benzo(g,h,i)perylene	Aromatics	PAHs	0.955
Tricosane	Alkanes	n-alkane	0.985	Toluene	Aromatics	SRAs	0.99
Tetracosane	Alkanes	n-alkane	0.992	Ethylbenzene	Aromatics	SRAs	0.965
Pentacosane	Alkanes	n-alkane	0.96	m-Xylene	Aromatics	SRAs	0.997
Hexacosane	Alkanes	n-alkane	0.974	o-Xylene	Aromatics	SRAs	0.979
Heptacosane	Alkanes	n-alkane	0.987	p-Xylene	Aromatics	SRAs	0.987
Octacosane	Alkanes	n-alkane	0.998	1,3,5-Trimethylbenzen	Aromatics	SRAs	0.976
Nonacosane	Alkanes	n-alkane	0.985	1,2,4-Trimethylbenzen	Aromatics	SRAs	0.999

Compounds	Category	Subcategory	R^2	compounds	Category	Subcategory	R^2
Triacontane	Alkanes	n-alkane	0.981	1,2,3-Trimethylbenzen	Aromatics	SRAs	0.962
Cyclohexane,heptyl-	Alkanes	cycloalkane	0.979	Styrene	Aromatics	SRAs	0.987
Cyclopentane,butyl-	Alkanes	cycloalkane	0.988	Benzene, (1-methylethyl)-	Aromatics	SRAs	0.981
Cyclohexane,pentyl-	Alkanes	cycloalkane	0.991	Benzaldehyde	O-components	aldehydes	0.991
Cyclohexanone	O-components	ketones	0.996	Benzene, nitro-	N-components	N-components	0.993

Table S5 Surrogate compounds (n-alkanes) for SOA yields of different Bin from Zhao et al., 2014

Bin		B_{12}	B_{13}	B_{14}	B_{15}	B_{16}	B_{17}	B_{18}	B_{19}	B_{20}	B_{21}	B_{22}
Surrogate compounds (n-alkanes) for SOA yields	Unspeciated b-alkanes compounds	C_{10}	C_{11}	C_{12}	C_{13}	C_{14}	C_{15}	C_{16}	C_{17}	C_{18}	C_{19}	C_{20}
	Unspeciated cyclic compounds	C_{12}	C_{13}	C_{14}	C_{15}	C_{16}	C_{17}	C_{18}	C_{19}	C_{20}	C_{21}	C_{22}

Supplementary Figure

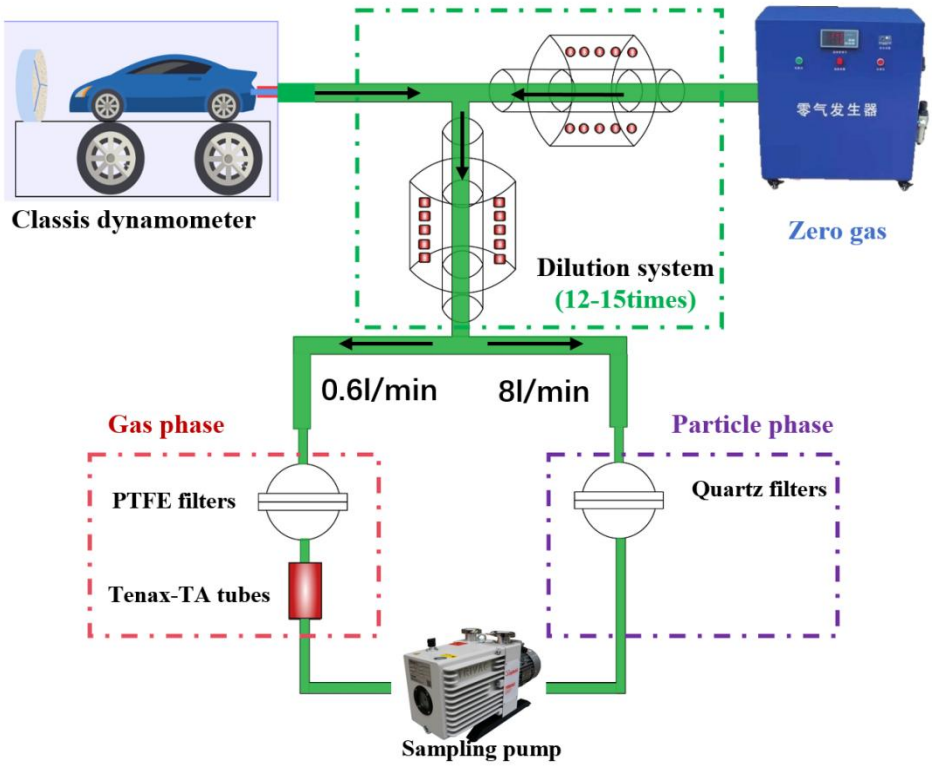

Fig. S1 The Schematic of the dynamometer experiments.

Fig. S2 The sampling field in classis dynamometer in our study.

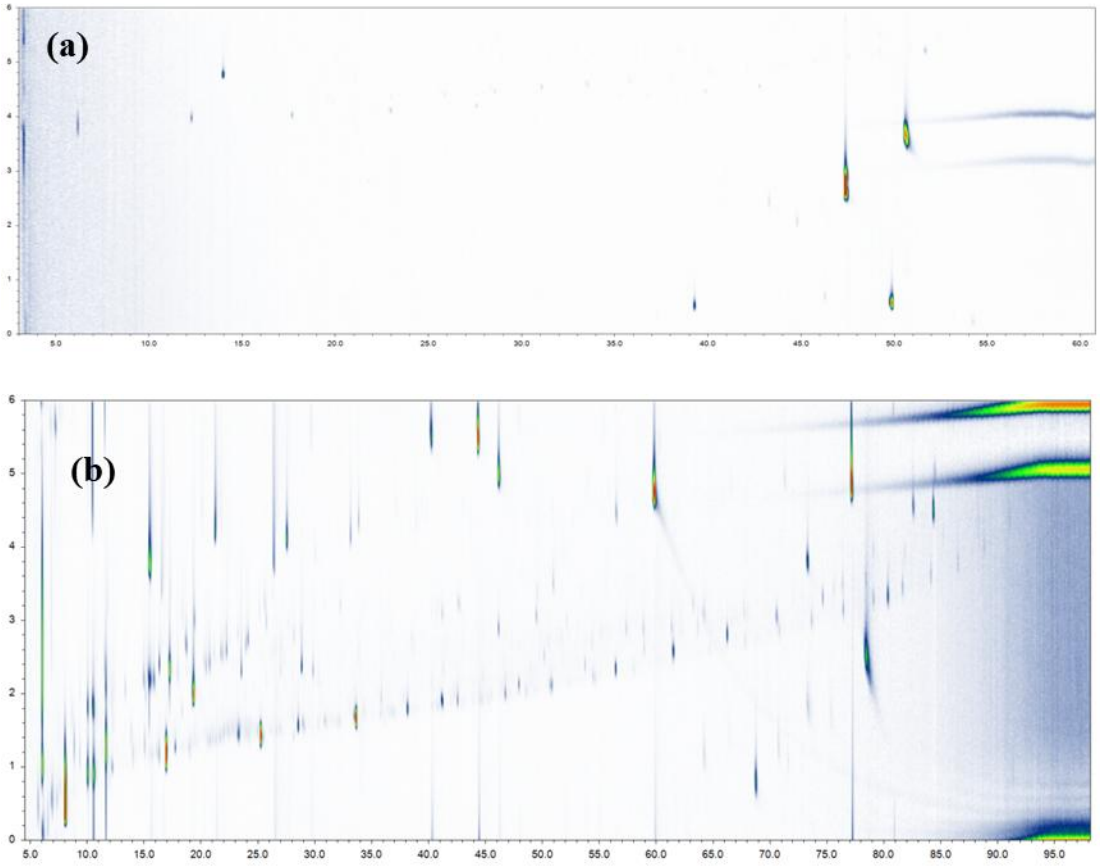

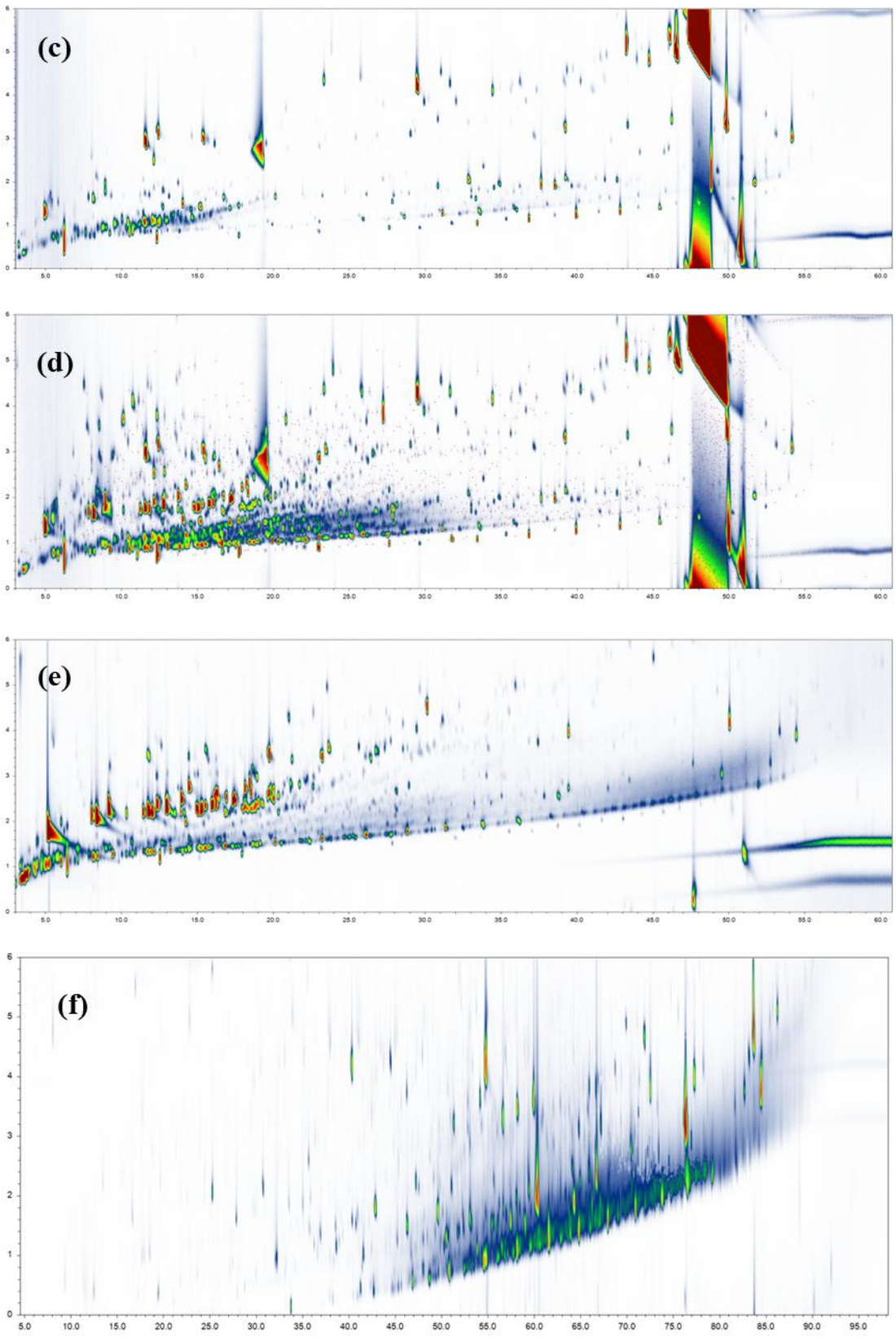
(c)
(d)
(e)
(f)

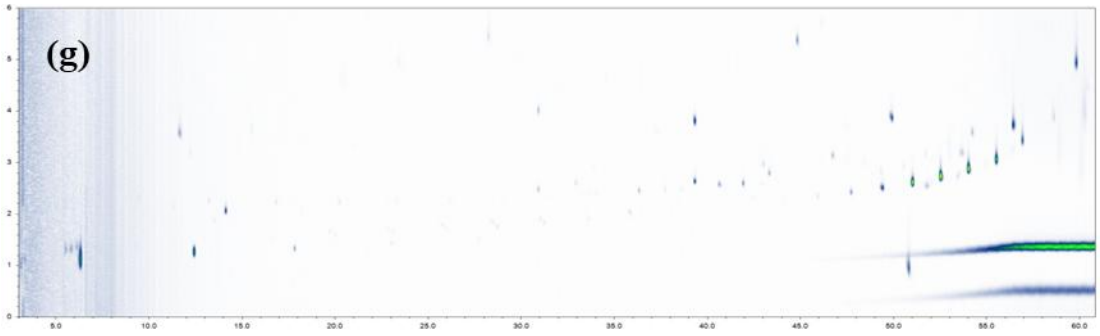

Fig. S3 The typical chromatogram of (a) blank sample; (b) field blank; (c) and (d) were the gas sample of gasoline vehicle and diesel vehicle; (e) and (f) were the particle sample of gasoline vehicle and diesel vehicle; (g) the second tubes of breakthrough experiment.

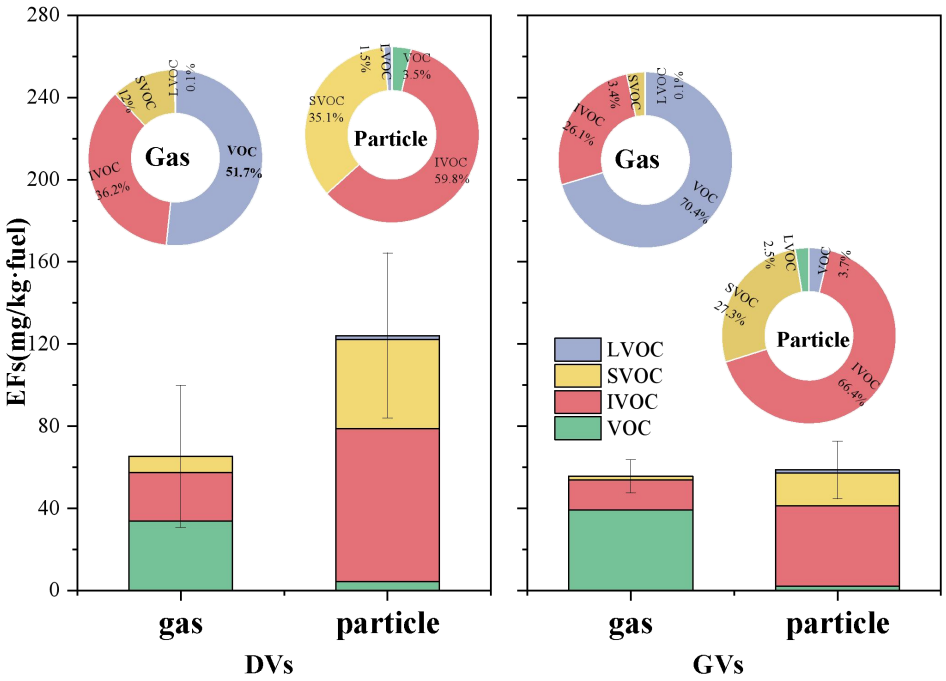

Fig. S4 Characteristics of total organic component EFs for China VI diesel and gasoline Vehicles in both gas and particle phase.

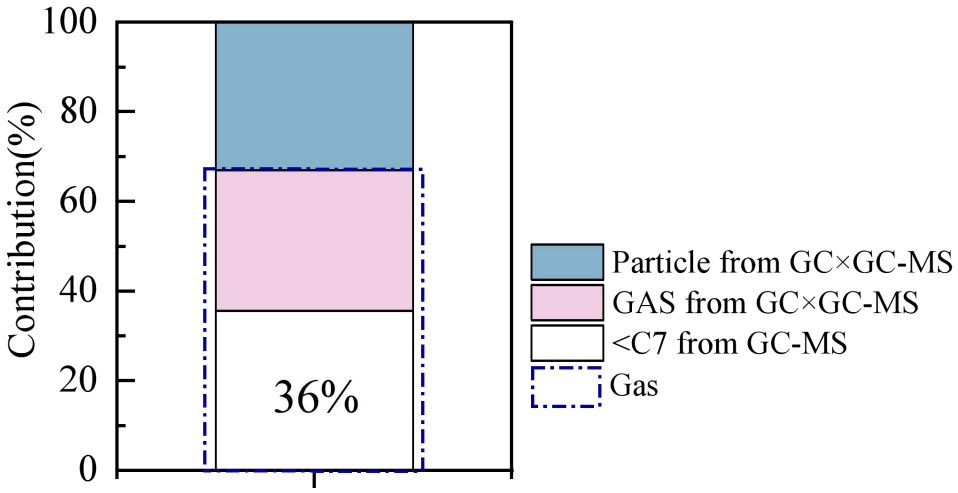

Fig. S5 The merging data of China VI GVs from GC × GC-MS and GCMS (VOCs data of GVs analyzed by GCMS , refer to published literature : Liu et al., 2024).

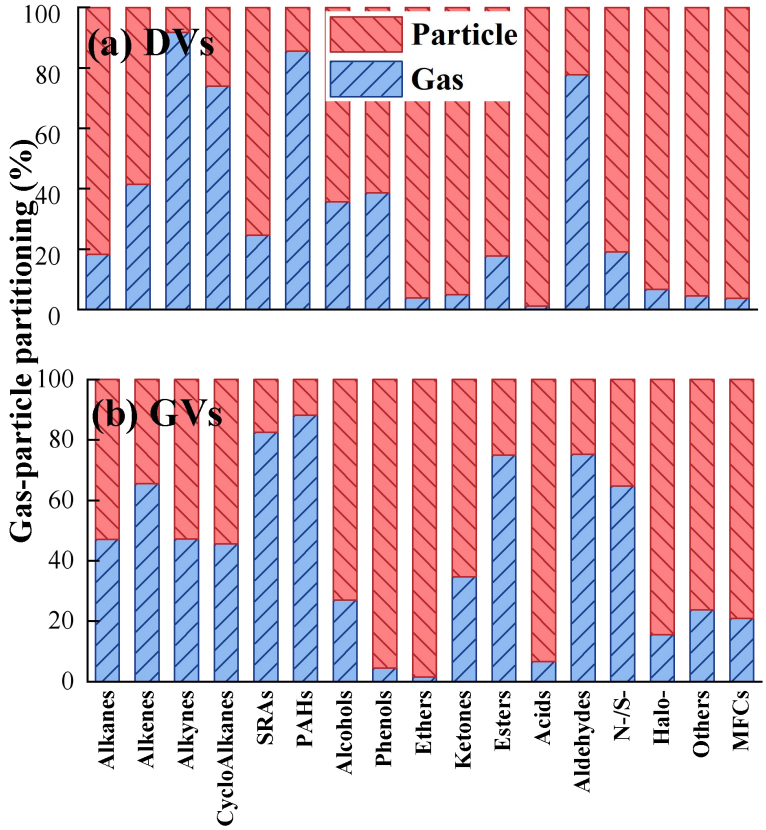

Fig. S6 The Gas-particle partitioning of S/IVOCs in China VI vehicles tailpipe emissions. (a) Diesel vehicles; (b) Gasoline vehicles.

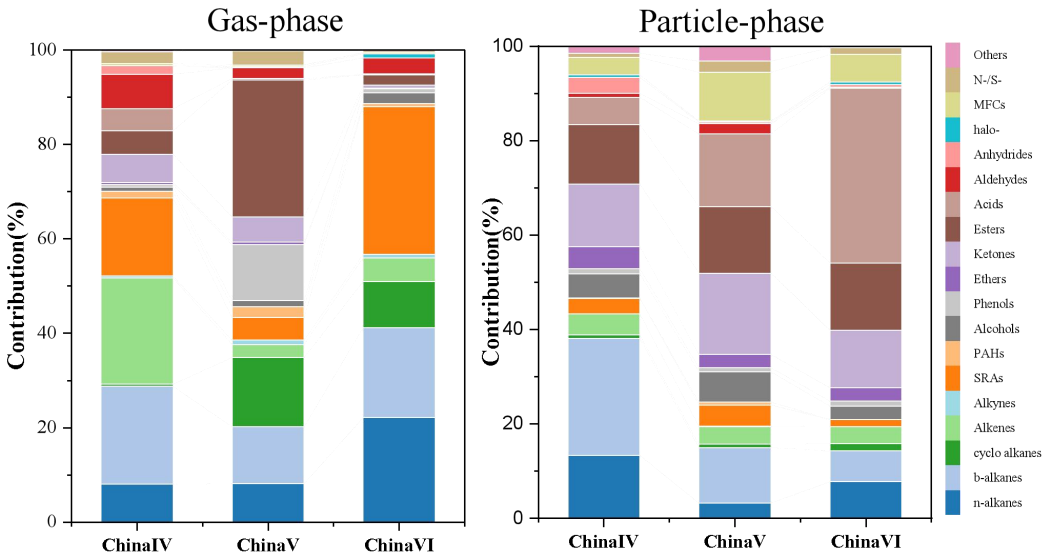

Fig. S7 The composition of I/SVOCSs emissions from Diesel Vehicle under different emission standard in both gas and particle phase.

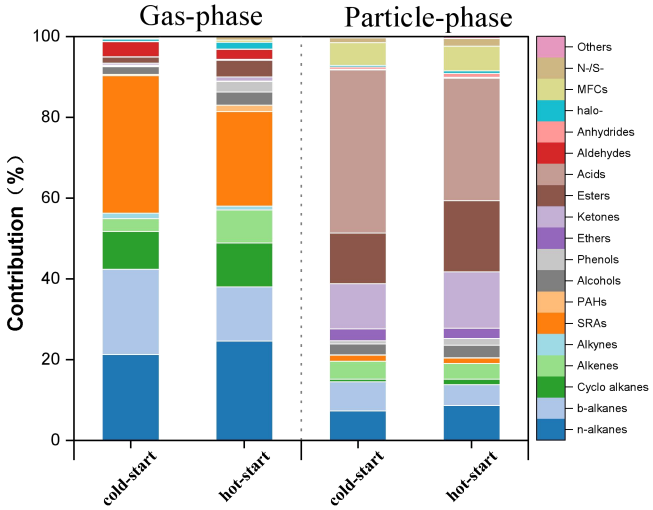

Fig. S8 The composition of I/SVOCSs emissions from China VI Diesel Vehicle under different start model in both gas and particle phase.

References

Huo Y, Guo Z, Li Q, Wu D, Ding X, Liu A, Huang D, Qiu G, Wu M, Zhao Z, Sun H, Song W, Li X, Chen Y, Wu T, Chen J (2021). Chemical fingerprinting of HULIS in particulate matters emitted from residential coal and biomass combustion. Environmental Science & Technology, 55(6): 3593–3603 doi:10.1021/acs.est.0c08518

Lin P, Fleming L T, Nizkorodov S A, Laskin J, Laskin A (2018). Comprehensive molecular characterization of atmospheric brown carbon by high resolution mass spectrometry with electrospray and atmospheric pressure photoionization. Analytical Chemistry, 90(21): 12493–12502 doi:10.1021/acs.analchem.8b02177

Lu Q, Zhao Y, Robinson A L (2018). Comprehensive organic emission profiles for gasoline, diesel, and gas-turbine engines including intermediate and semi-volatile organic compound emissions. Atmospheric Chemistry and Physics, 18(23): 17637–17654 doi:10.5194/acp-18-17637-2018

Song K, Guo S, Gong Y, Lv D, Wan Z, Zhang Y, Fu Z, Hu K, Lu S (2023a). Non-target scanning of organics from cooking emissions using comprehensive two-dimensional gas chromatography-mass spectrometer (GC×GC-MS). Applied Geochemistry, 151: 105601 doi:10.1016/j.apgeochem.2023.105601

Song K, Tang R, Zhang J, Wan Z, Zhang Y, Hu K, Gong Y, Lv D, Lu S, Tan Y, Zhang R, Li A, Yan S, Yan S, Fan B, Zhu W, Chan C K, Yao M, Guo S (2023b). Molecular fingerprints and health risks of smoke from home-use incense burning. Atmospheric Chemistry and Physics, 23(21): 13585–13595 doi:10.5194/acp-23-13585-2023

Song K, Yang X, Wang Y, Wan Z, Wang J, Wen Y, Jiang H, Li A, Zhang J, Lu S, Fan B, Guo S, Ding Y (2023c). Addressing new chemicals of emerging concern (CECs) in an indoor office. Environment International, 181: 108259 doi:10.1016/j.envint.2023.108259

Zhang Y, Wang X, Wen S, Herrmann H, Yang W, Huang X, Zhang Z, Huang Z, He Q, George C (2016). On-road vehicle emissions of glyoxal and methylglyoxal from tunnel tests in urban Guangzhou, China. Atmospheric Environment, 127: 55–60 doi:10.1016/j.atmosenv.2015.12.017

Zhao Y, Hennigan C J, May A A, Tkacik D S, De Gouw J A, Gilman J B, Kuster W C, Borbon A, Robinson A L (2014). Intermediate-volatility organic compounds: A large source of secondary organic aerosol. Environmental Science & Technology, 48(23): 13743–13750 doi:10.1021/es5035188